The Astrophysical Journal, 903:33 (12pp), 2020 November 1 https://doi.org/10.3847/1538-4357/abb9b7

A Multilevel Empirical Bayesian Approach to Estimating the Unknown Redshifts of 1366 BATSE Catalog Long-duration Gamma-Ray Bursts

Joshua A. Osborne[1], Amir Shahmoradi[1,2], and Robert J. Nemiroff[3]
[1] Department of Physics, The University of Texas, Arlington, TX 76010, USA; joshua.osborne@mavs.uta.edu, shahmoradi@utexas.edu
[2] Data Science Program, College of Science, The University of Texas, Arlington, TX 76010, USA
[3] Department of Physics, Michigan Technological University, Houghton, MI 49931, USA; nemiroff@mtu.edu
Received 2019 March 16; revised 2020 August 25; accepted 2020 September 6; published 2020 October 29

Abstract

We present a catalog of probabilistic redshift estimates for 1366 individual Long-duration Gamma-ray Bursts (LGRBs) detected by the Burst And Transient Source Experiment (BATSE). This result is based on a careful selection and modeling of the population distribution of 1366 BATSE LGRBs in the five-dimensional space of redshift and the four intrinsic prompt gamma-ray emission properties: the isotropic 1024 ms peak luminosity ($L_{\rm iso}$), the total isotropic emission ($E_{\rm iso}$), the spectral peak energy ($E_{\rm pz}$), as well as the intrinsic duration (T_{90z}), while carefully taking into account the effects of sample incompleteness and the LGRB-detection mechanism of BATSE. Two fundamental plausible assumptions underlie our purely probabilistic approach: (1) LGRBs trace, either exactly or closely, the cosmic star formation rate, with a possibility of the excess rates of LGRBs in the nearby universe, and (2) the joint four-dimensional distribution of the aforementioned prompt gamma-ray emission properties is well described by a multivariate log-normal distribution. Our modeling approach enables us to constrain the redshifts of individual BATSE LGRBs to within 0.36 and 0.96 average uncertainty ranges at 50% and 90% confidence levels, respectively. Our redshift predictions are completely at odds with the previous redshift estimates of BATSE LGRBs that were computed via the proposed phenomenological high-energy relations, specifically, the apparently strong correlation of LGRBs' peak luminosity with the spectral peak energy, lightcurve variability, and spectral lag. The observed discrepancies between our predictions and the previous works can be explained by the strong influence of detector threshold and sample incompleteness in shaping these phenomenologically proposed high-energy correlations in the literature. Finally, we also discuss the potential effects of an excess cosmic rate of LGRBs at low redshifts and the possibility of a luminosity evolution of LGRBs on our results.

Unified Astronomy Thesaurus concepts: Gamma-ray bursts (629); Gamma-ray detectors (630); Astronomy data modeling (1859); Astronomy data analysis (1858); Luminosity function (942); Catalogs (205); Markov chain Monte Carlo (1889); Astronomical simulations (1857); Bayesian statistics (1900); Hierarchical models (1925)

Supporting material: machine-readable table

1. Introduction

Throughout almost a decade of continuous operation, the Burst And Transient Source Experiment (BATSE) on board the now-defunct Compton Gamma-ray Observatory (Meegan et al. 1992) detected more than 2700 Gamma-ray Bursts (GRBs). The BATSE catalog of GRBs provided the first solid evidence for the existence of at least two classes of GRBs: the short-hard (SGRBs) and the long-soft (LGRBs; e.g., Kouveliotou et al. 1993).

Traditionally, new GRB events have been classified into one of the two classes based on a sharp cutoff on the bimodal distribution of the observed duration (T_{90}) of the prompt gamma-ray emission, generally set to $T_{90} \sim 2$–$3[s]$. However, the dependence of the observed duration of GRBs on the gamma-ray energy and the detector's specifications (e.g., Fenimore et al. 1995; Nemiroff 2000; Qin et al. 2012) has prompted many studies in search of less-biased alternative methods of GRB classification, typically based on a combination of the prompt gamma-ray and afterglow emissions as well as the host galaxy's properties (e.g., Gehrels et al. 2009; Zhang et al. 2009; Shahmoradi & Nemiroff 2010; Goldstein et al. 2011; Shahmoradi & Nemiroff 2011a; Zhang et al. 2012; Shahmoradi 2013a, 2013b; Shahmoradi & Nemiroff 2014, 2015; Lü et al. 2014) or based on the prompt emission spectral correlations in conjunction with the traditional method of classification (e.g., Qin & Chen 2013).

Ideally, the classification of GRBs should be independent of their cosmological distances from Earth and free from potential sample biases due to detector specifications, selection effects, and sample incompleteness and should solely rely on their intrinsic properties. Such classification methods are still missing in the GRB literature and hard to devise, mainly due to the lack of a homogenously detected, sufficiently large catalog of GRBs with measured redshifts.

Several studies have already attempted to estimate the unknown redshifts of GRBs based on the apparently strong phenomenological correlations observed between some of the spectral and temporal prompt gamma-ray emission properties of GRBs. The most prominent class of such relations are the apparently strong correlations of the intrinsic brightness measures of the prompt gamma-ray emission (e.g., the total isotropic emission, $E_{\rm iso}$, and the peak 1024 ms luminosity, $L_{\rm iso}$) with other spectral or temporal properties of GRBs, such as hardness as measured by the intrinsic spectral peak energy $E_{\rm pz}$ (e.g., Yonetoku et al. 2004, 2014), lightcurve variability (e.g., Fenimore & Ramirez-Ruiz 2000; Reichart et al. 2001), and spectral lag (e.g., Schaefer et al. 2001), or based on a

combination of such relationships (e.g., Xiao & Schaefer 2009; Dainotti et al. 2019).

These methods, however, can lead to incorrect or highly biased estimates of the unknown redshifts of GRBs if the observed high-energy correlations are constructed from a small sample of GRBs (typically the brightest events) with measured redshifts. Such small samples are often collected from multiple heterogeneous surveys and may neither represent the entire population of observed GRBs (with or without measured redshift) nor represent the unobserved cosmic population. More importantly, the potential effects of detector threshold and sample incompleteness on them are poorly understood. Such biases manifest themselves in redshift estimates that are inconsistent with estimates from other methods, examples of which have been already reported by several authors (e.g., Guidorzi 2005; Ashcraft & Schaefer 2007; Rizzuto et al. 2007; Bernardini et al. 2014).

The selection effects in the detection, analysis, and redshift measurements of GRBs and their potential effects on the observed phenomenological high-energy correlations have been already extensively studied individually, in isolation from other correlations, (e.g., Petrosian & Lee 1996; Lloyd & Petrosian 1999; Petrosian et al. 1999; Lloyd et al. 2000; Hakkila et al. 2003; Nakar & Piran 2004; Band & Preece 2005; Butler et al. 2007; Ghirlanda et al. 2008; Nava et al. 2008; Butler et al. 2009, 2010; Shahmoradi & Nemiroff 2009, 2011a, 2011b; Shahmoradi 2013b; Dainotti et al. 2015; Petrosian et al. 2015). However, an ultimate resolution to the problem of estimating the unknown redshifts of GRBs in catalogs requires simultaneous multidimensional modeling of the intrinsic population distribution of GRB attributes, subject to the effects of detector threshold and sample incompleteness on their joint observed distribution (e.g., Butler et al. 2010; Shahmoradi 2013a; Shahmoradi & Nemiroff 2014, 2015).

Building upon our previous studies in Shahmoradi (2013b, 2013a) and Shahmoradi & Nemiroff (2015) and motivated by the existing gap in the knowledge of the redshifts of LGRBs in the BATSE catalog (e.g., Paciesas et al. 1999; Goldstein et al. 2013), which as of 2020, constitutes the largest catalog of homogenously detected GRBs, here we present a methodology and modeling approach to constraining the redshifts of 1366 BATSE LGRBs. Despite lacking complete knowledge of the true cosmic rate and redshift distribution of LGRBs, we show that it is possible to constrain the redshifts of individual BATSE LGRBs to within uncertainty ranges of width 0.7 and 1.7, on average, at 50% and 90% confidence levels, respectively. Our methodology relies on two plausible assumptions that are strongly supported by currently existing evidence: (1) LGRBs trace the cosmic star formation rate (SFR) or a metallicity-corrected SFR (e.g., Butler et al. 2010; Pontzen et al. 2010) and (2) the joint distribution of the four main prompt gamma-ray-emission properties of LGRBs is well described by a multivariate log-normal distribution (e.g., Shahmoradi 2013a; Shahmoradi & Nemiroff 2015). The presented work also paves the way toward a detector-independent, minimally biased phenomenological classification method for GRBs solely based on the intrinsic prompt gamma-ray data of individual events. Without the assumption of a multivariate log-normal distribution, it becomes essentially impossible to infer the redshifts due to our limited knowledge of observed BATSE LGRB redshifts. We acknowledge the potential impact of such assumption on our results and discuss it further in Section 4.

In the following sections, we present an attempt to further uncover some of the tremendous amounts of useful, yet unexplored, information that is still buried in this seemingly archaic catalog of GRBs. Toward this, we devote Section 2 of this manuscript to the development of the redshift inference methodology, which includes a discussion of the data collection procedure in Section 2.1, a generic description of our probabilistic modeling approach via a toy problem in Section 2.2, followed by detailed descriptions of the proposed methodology for estimating redshifts in Section 2.3, the cosmic SFR assumptions underlying our model in Section 2.4, the construction of an LGRB world model in Section 2.5, and a review of the BATSE LGRB-detection algorithm and our approach to modeling the BATSE LGRB sample incompleteness in Section 2.6. The predictions of the model are presented in Section 3, followed by a discussion of the implications of the results, comparison with previous independent redshift estimates, and possible reasons for the observed discrepancies between the results of this study and the previous studies in Section 4.

2. Methods

2.1. BATSE LGRB Data

Fundamental to our inference problem is the issue of obtaining a data set of BATSE LGRBs that is minimally biased and representative of the population distribution of LGRBs detectable by the BATSE Large Area Detectors (LADs). The traditional method of GRB classification based on a sharp cutoff line on the observed duration variable T_{90} set at 2–3[s] (Kouveliotou et al. 1993) has been shown to be insufficient for an unbiased classification because the duration distributions of LGRBs and SGRBs have significant overlap (e.g., Butler et al. 2010; Shahmoradi 2013a; Shahmoradi & Nemiroff 2015). Instead, we follow the multivariate fuzzy classification approach of Shahmoradi (2013a) and Shahmoradi & Nemiroff (2015) to segregate the two populations of BATSE LGRBs and SGRBs based on their estimated observed spectral peak energies (E_p) from Shahmoradi & Nemiroff (2010) and T_{90} from the current BATSE catalog (Goldstein et al. 2013). This leads us to a sample of 1366 LGRBs versus 565 SGRBs in the current BATSE catalog. We refer the interested reader to Shahmoradi (2013a) and Shahmoradi & Nemiroff (2015) for extensive details of the classification procedure.

For our analysis, we also compute, as detailed in Shahmoradi (2013a) and Shahmoradi & Nemiroff (2015), the 1024 [ms] bolometric peak flux ($P_{\rm bol}$) and the bolometric fluence ($S_{\rm bol}$) of these events from the current BATSE catalog for inclusion in the analysis, in addition to E_p and T_{90}. Taking into account the measurement uncertainties associated with each BATSE event, we can therefore, represent the ith event, $\boldsymbol{D}^{g}_{\rm obs,i}$, in the BATSE catalog by an a priori "known" measurement uncertainty model, $M^{g}_{\rm inois}$, that together with its "known" parameters, $M^{g}_{\rm inois^g}$, determine the joint four-dimensional probability density function of the observed attributes of the event,

$$\pi(\boldsymbol{D}^{g}_{\rm obs,i}|M^{g}_{\rm inois}, M^{g}_{\rm inois^g}) \propto M^{g}_{\rm inois}(\boldsymbol{D}^{g}_{\rm obs,i}, M^{g}_{\rm inois^g}). \quad (1)$$

The modes of these uncertainty models are essentially the values reported in the BATSE catalog and Shahmoradi &

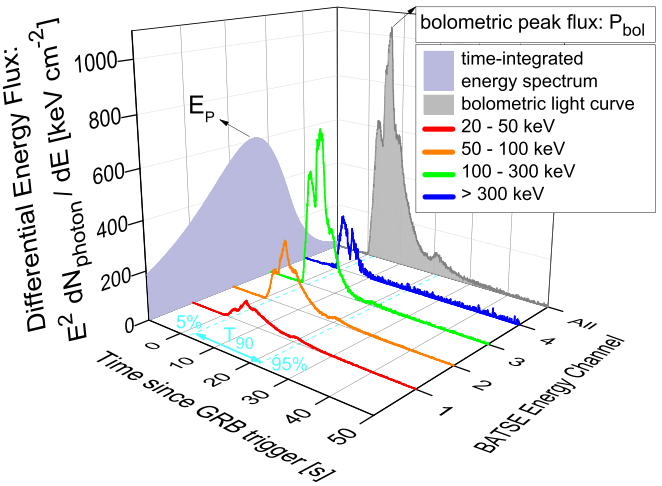

Figure 1. Example GRB lightcurve (BATSE trigger 1085) illustrating the four main LGRB properties used as input observational data in this study (Equation (2)): the observed 1 s bolometric peak energy flux ($P_{\rm bol}$), the observed total energy fluence ($S_{\rm bol}$), the observed spectral peak energy ($E_{\rm p}$), and the observed duration within which the GRB event releases 90% of its gamma-ray emission (T_{90}). The four red, orange, green, and blue-colored lines represent the total energy flux received, as a function of time, in each of the four BATSE main energy channels.

Nemiroff (2010),

$$\widehat{\boldsymbol{D}}^{\rm g}_{\rm obs,i} = [\widehat{P}_{\rm bol,i}, \widehat{S}_{\rm bol,i}, \widehat{E}_{\rm p,i}, \widehat{T}_{90,i}], \tag{2}$$

The entire BATSE data set of 1366 LGRB event attributes is then represented by the collection of pairs of such uncertainty models and their parameters,

$$\mathcal{D}^{\rm g}_{\rm obs} = \{(M^{\rm g}_{\rm inois}, M^{\rm g}_{\rm inois^g}):\ 1 \leqslant i \leqslant 1366\} \tag{3}$$

Note that throughout this manuscript, the appearance of "g" as a superscript solely indicates that the quantity relates to or depends on the four main physical LGRB properties considered in this study, excluding any redshift (z) information.

The BATSE catalog observations appear to have been reported with the assumption that the measurement uncertainty models for all events are multivariate normal distributions, with their mean vectors being the values reported in the catalog and their covariance matrices being diagonal, with the diagonal elements representing the square of the 1–σ errors reported in the catalog.

In sum, our observational data comprises the four main prompt gamma-ray emission properties of LGRBs as described by Equations (1) and (2) and illustrated by Figure 1. $P_{\rm bol}$, as in Equation (2), is, however, a conventionally defined measure of the peak brightness and peripheral to and highly correlated with the more fundamental GRB attribute, $S_{\rm bol}$, its inclusion in our GRB world model is essential as it determines, together with $E_{\rm p}$, the peak photon flux, $P_{\rm ph}$, in 50–300 [keV] range, based upon which BATSE LADs generally triggered on LGRBs.

2.2. The Multilevel Empirical Bayesian Approach

Except for a handful of GRB events, the entire BATSE catalog of GRBs lack any redshift or distance information. Knowledge of individual redshifts is absolutely necessary for accurate cosmographic studies of LGRBs. Essentially, our missing-redshift-data problem for each LGRB reduces to a set of four equations,

$$\begin{aligned} L_{\rm iso} &= 4\pi \times d_L(z)^2 \times P_{\rm bol},\\ E_{\rm iso} &= 4\pi \times d_L(z)^2 \times S_{\rm bol}/(z+1),\\ E_{\rm pz} &= E_{\rm p} \times (z+1),\\ T_{90z} &= T_{90}/(z+1)^{\alpha}, \end{aligned} \tag{4}$$

that exactly determine the intrinsic properties of LGRBs: the 1024 [ms] isotropic peak luminosity ($L_{\rm iso}$), the total isotropic emission ($E_{\rm iso}$), the intrinsic spectral peak energy ($E_{\rm pz}$), and the intrinsic duration (T_{90z}). These four properties are collectively represented by

$$\boldsymbol{D}^{\rm g}_{\rm int,i} = [L_{\rm iso,i}, E_{\rm iso,i}, E_{\rm pz,i}, T_{90z,i}]. \tag{5}$$

The term $d_L(z)$ in Equation (4) represents the luminosity distance,

$$d_L(z) = \frac{C}{H_0}(1+z)\int_0^z dz'[(1+z')^3\Omega_M + \Omega_\Lambda]^{-1/2}, \tag{6}$$

and the exponent $\alpha = 0.66$ in the mapping of T_{90} to T_{90z} takes into account the cosmological time dilation as well as an energy-band correction (i.e., K-correction) of the form $(1+z)^{-0.34}$ to the observed durations (e.g., Gehrels et al. 2006). Throughout this work, we assume a flat ΛCDM cosmology, with parameters set to $h = 0.70$, $\Omega M = 0.27$, and $\Omega_\Lambda = 0.73$ (Jarosik et al. 2011). Also, the parameters C and $H_0 = 100h$ [km s^{-1} MPc^{-1}] stand for the speed of light and the Hubble constant, respectively. Equations (4) can be linearized by taking the logarithms of both sides, leading to

$$\begin{aligned} \log(L_{\rm iso}) &= \log(P_{\rm bol}) + 2\log(d_L) + \log(4\pi),\\ \log(E_{\rm iso}) &= \log(S_{\rm bol}) + 2\log(d_L) + \log(4\pi) - \log(z+1),\\ \log(E_{\rm pz}) &= \log(E_{\rm p}) + \log(z+1),\\ \log(T_{90z}) &= \log(T_{90}) - \alpha\log(z+1). \end{aligned} \tag{7}$$

More concisely, we can write the four Equations (7) for the ith GRB event as a single equation,

$$\log(\boldsymbol{D}^{\rm g}_{\rm int,i}) = \log(\boldsymbol{D}^{\rm g}_{\rm obs,i}) + \mathcal{F}(z_i), \tag{8}$$

where $\mathcal{F}(z_i)$ describes the mapping from the observer to the rest frame of the GRB given its known redshift, z_i. This simple equation deserves some deliberations. Despite its simplicity, this single equation is algebraically unsolvable for almost any BATSE catalog GRB as it contains two unknowns ($\boldsymbol{D}^{\rm g}_{\rm int,i}$, z_i).

Although Equation (8) is algebraically degenerate, the two unknowns of the equation can still be constrained probabilistically. To understand how this is possible, consider the following simple toy problem.

Without loss of generality, suppose the observed properties of individual BATSE LGRBs are exactly known, with no measurement error, as illustrated by the individual blue-colored vertical lines in the bottom plot of Figure 2. The corresponding redshifts of these events, (represented by the black lines in the middle plot of Figure 2) are, however, unknown, and we wish to estimate them. Although we have no knowledge of the joint population distribution of the intrinsic properties of LGRBs, illustrated by the red distribution on the top plot of Figure 2, there are strong arguments in favor of these properties being potentially well described by a four-dimensional multivariate log-normal distribution, $\mathcal{N}(\boldsymbol{\mu}, \boldsymbol{\Sigma})$, in the space of $L_{\rm iso}$, $E_{\rm iso}$,

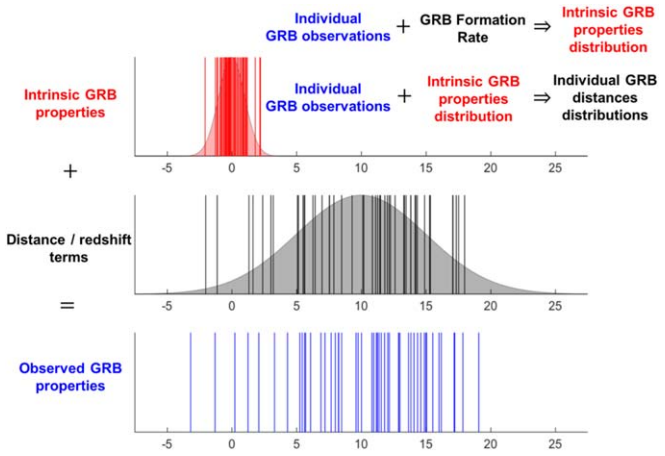

Figure 2. Schematic illustration of the multilevel empirical Bayesian approach to estimating the unknown redshifts of BATSE LGRBs (the gray lines). The process of inferring the redshifts involves two separate steps. At the first stage, we convolve the observed BATSE LGRB properties (the individual blue lines) with prior knowledge of the overall cosmic redshift distribution of LGRBs (the gray distribution) to infer the unknown parameters of the joint population distribution of the intrinsic properties of LGRBs (the red distribution). Then, we combine the inferred best-fit model for the distribution of the intrinsic properties of LGRBs with the observed LGRB properties to estimate the unknown redshifts of individual BATSE LGRBs at the second stage of the inference process. The red lines in the figure represent the unknown true intrinsic properties of individual BATSE LGRBs, whose knowledge is not essential in this redshift estimation workflow discussed above.

$E_{\rm pz}$, and T_{90z} (Shahmoradi 2013a; Shahmoradi & Nemiroff 2015). Here, $\boldsymbol{\mu}$ and $\boldsymbol{\Sigma}$ represent the mean and the covariance matrix of the multivariate log-normal distribution, respectively.

We now reach the crucial step in the inference process: despite the complete lack of information about the redshifts of BATSE LGRBs, we can use the existing prior knowledge about the overall cosmic redshift distribution of LGRBs to integrate over all possible redshifts for each observed LGRB in the BATSE catalog to infer a range of plausible values for the intrinsic properties of the corresponding LGRB. These individually computed probability density functions (PDFs) of the intrinsic properties can be then used to infer the unknown parameters $(\boldsymbol{\mu}, \boldsymbol{\Sigma})$ of the joint population distribution of the intrinsic properties of LGRBs (i.e., the multivariate log-normal distribution).

Once $(\boldsymbol{\mu}, \boldsymbol{\Sigma})$ are constrained, we can use the inferred population distribution of the intrinsic LGRB properties together with the observed properties to estimate the redshifts of individual BATSE LGRBs, independently of each other. The estimated redshifts can again be used to further constrain $\mathcal{N}(\boldsymbol{\mu}, \boldsymbol{\Sigma})$, which will then result in even tighter estimates for the individual redshifts of BATSE LGRBs. This recursive progress can practically continue until convergence to a set of fixed individual redshift estimates occurs.

At first glance, this simple semi-Bayesian mathematical approach may sound like magic and perhaps, too good to be true. Sometimes it is. However, as we later explain in Section 4, it can also lead to reasonably accurate results if some conditions regarding the problem and the observational data set are satisfied.

2.3. The Cosmic Rates of LGRBs

More formally, we model the process of LGRB observation as a nonhomogeneous Poisson process whose mean rate parameter is the "censored" cosmic LGRB rate, $\mathcal{R}_{\rm cen}$. Representing each LGRB by

$$\boldsymbol{D}_{\rm int,i} = \{\boldsymbol{D}^{\rm g}_{\rm int,i}, z_{\rm i}\},\ 1 \leqslant i \leqslant 1366, \tag{9}$$

where $\boldsymbol{D}^{\rm g}_{\rm int,i}$ is defined by Equation (5), we compute the probability of occurrence of each BATSE LGRB event in the five-dimensional attributes space, $\Omega(\boldsymbol{D}_{\rm int})$, of z, $L_{\rm iso}$, $E_{\rm iso}$, $E_{\rm pz}$, T_{90z}, as a function of the parameters, $\boldsymbol{\theta}_{\rm cen}$, of the observed LGRB rate model, $\mathcal{R}_{\rm cen}$,

$$\pi(\boldsymbol{D}_{\rm int,i}|\mathcal{R}_{\rm cen}, \boldsymbol{\theta}_{\rm cen}) \propto \mathcal{R}_{\rm cen}(\boldsymbol{D}_{\rm int,i}, \boldsymbol{\theta}_{\rm cen}), \tag{10}$$

where $\mathcal{R}_{\rm cen}$ represents the BATSE-censored rate of LGRB occurrence in the universe (due to the BATSE detection efficiency limitations as detailed in Section 2.6). This equation can be further expanded in terms of BATSE detection efficiency function, $\eta_{\rm eff}$, and the true cosmic LGRB rate, $\mathcal{R}_{\rm tru}$, as

$$\begin{aligned}\frac{dN_{\rm obs}}{d\boldsymbol{D}_{\rm int}} &= \mathcal{R}_{\rm cen}(\boldsymbol{D}_{\rm int}, \boldsymbol{\theta}_{\rm cen}),\\ &= \eta_{\rm eff}(\boldsymbol{D}_{\rm int}, \boldsymbol{\theta}_{\rm eff}) \times \mathcal{R}_{\rm tru}(\boldsymbol{D}_{\rm int}, \boldsymbol{\theta}_{\rm tru})\end{aligned} \tag{11}$$

for a given set of input intrinsic LGRB attributes, $\boldsymbol{D}_{\rm int}$, with $\boldsymbol{\theta}_{\rm cen} = \{\boldsymbol{\theta}_{\rm eff}, \boldsymbol{\theta}_{\rm tru}\}$ as the set of the parameters of our models for the BATSE detection efficiency and the intrinsic cosmic LGRB rate, respectively. Assuming no systematic evolution of LGRB characteristics with redshift, which is a plausible assumption supported by independent studies (e.g., Butler et al. 2010; hereafter B10), the intrinsic LGRB rate itself can be written as

$$\begin{aligned}\frac{dN_{\rm int}}{d\boldsymbol{D}_{\rm int}} &= \mathcal{R}_{\rm tru}(\boldsymbol{D}_{\rm int}, \boldsymbol{\theta}_{\rm tru})\\ &= \mathcal{R}^{\rm g}_{\rm tru}(\boldsymbol{D}^{\rm g}_{\rm int}, \boldsymbol{\theta}^{\rm g}_{\rm tru}) \times \frac{\dot{\zeta}(z, \boldsymbol{\theta}_z) dV/dz}{(1+z)},\end{aligned} \tag{12}$$

with $\boldsymbol{\theta}_{\rm tru} = \{\boldsymbol{\theta}^{\rm g}_{\rm tru}, \boldsymbol{\theta}_z\}$, where $\mathcal{R}^{\rm g}_{\rm tru}$ is a statistical model, with $\boldsymbol{\theta}^{\rm g}_{\rm tru}$ denoting its parameters that describe the population distribution of LGRBs in the four-dimensional attributes space of $\boldsymbol{D}^{\rm g}_{\rm int} = [L_{\rm iso}, E_{\rm iso}, E_{\rm pz}, T_{90z}]$, and the term $\dot{\zeta}(z, \boldsymbol{\theta}_z)$ represents the comoving rate density model of LGRBs with the set of parameters $\boldsymbol{\theta}_z$, while the factor $(1+z)$ in the denominator accounts for the cosmological time dilation. The comoving volume element per unit redshift, dV/dz, is given by (e.g., Winberg 1972; Peebles 1993)

$$\frac{dV}{dz} = \frac{C}{H_0} \frac{4\pi d_L^2(z)}{(1+z)^2[\Omega_{\rm M}(1+z)^3 + \Omega_\Lambda]^{1/2}}, \tag{13}$$

with d_L standing for the luminosity distance as given in Equation (6). If the three rate models, $(\dot{\zeta}, \eta_{\rm eff}, \mathcal{R}^{\rm g}_{\rm tru})$, and their parameters were known a priori, one could readily compute the PDFs of the set of unknown redshifts of all BATSE LGRBs,

$$\mathcal{Z} = \{z_{\rm i}:\ 1 \leqslant i \leqslant 1366\}, \tag{14}$$

as

$$\pi(\mathcal{Z}|\mathcal{D}^{\rm g}_{\rm obs}, \mathcal{R}_{\rm cen}, \boldsymbol{\theta}_{\rm cen}) \propto \int_{\Omega(\mathcal{D}^{\rm g}_{\rm int})} \mathcal{R}_{\rm cen}(\mathcal{Z}, \mathcal{D}^{\rm g}_{\rm int}{}^{*}, \boldsymbol{\theta}_{\rm cen})\, d\mathcal{D}^{\rm g}_{\rm int}{}^{*}, \quad (15)$$

where the integration is performed over all possible realizations, $\mathcal{D}^{\rm g}_{\rm int}{}^{*}$, of the BATSE LGRB data set given the measurement uncertainty models in Equation (3). For a range of possible parameter values, the redshift probabilities can be computed by marginalizing over the entire parameter space, $\Omega(\boldsymbol{\theta}_{\rm cen})$, of the model,

$$\pi(\mathcal{Z}|\mathcal{D}^{\rm g}_{\rm obs}, \mathcal{R}_{\rm cen}) = \int_{\Omega(\boldsymbol{\theta}_{\rm cen})} \pi(\mathcal{Z}|\mathcal{D}^{\rm g}_{\rm obs}, \mathcal{R}_{\rm cen}, \boldsymbol{\theta}_{\rm cen}) \times \pi(\boldsymbol{\theta}_{\rm cen}|\mathcal{D}^{\rm g}_{\rm obs}, \mathcal{R}_{\rm cen})\, d\boldsymbol{\theta}_{\rm cen}. \quad (16)$$

The problem, however, is that neither the rate models nor their parameters are known a priori. Even more problematic is the circular dependency of the posterior PDFs of $\mathcal{Z}$ and $\boldsymbol{\theta}_{\rm cen}$ on each other,

$$\pi(\boldsymbol{\theta}_{\rm cen} \mid \mathcal{D}^{\rm g}_{\rm obs}, \mathcal{R}_{\rm cen}) = \int_{\Omega(\mathcal{Z})} \pi(\boldsymbol{\theta}_{\rm cen}|\mathcal{Z}, \mathcal{D}^{\rm g}_{\rm obs}, \mathcal{R}_{\rm cen}) \times \pi(\mathcal{Z} \mid \mathcal{D}^{\rm g}_{\rm obs}, \mathcal{R}_{\rm cen})\, d\mathcal{Z}. \quad (17)$$

Therefore, we adopt the following methodology, which is reminiscent of the Empirical Bayes (Robbins 1985) and Expectation-Maximization algorithms (Dempster et al. 1977), to estimate the redshifts of BATSE LGRBs. First, we propose models for $(\dot{\zeta}, \eta_{\rm eff}, \mathcal{R}^{\rm g}_{\rm tru})$, whose parameters have yet to be constrained by observational data. Given the three rate models, we can then proceed to constrain the free parameters of the observed cosmic LGRB rate, $\mathcal{R}_{\rm cen}$, based on BATSE LGRB data.

The most appropriate fitting approach should take into account the observational uncertainties and any prior knowledge from independent sources. This can be achieved via the multilevel Bayesian methodology (e.g., Shahmoradi 2017) by constructing the likelihood function and the posterior PDF of the parameters of the model, while taking into account the uncertainties in observational data (e.g., Equation (61) in Shahmoradi 2017),

$$\pi(\boldsymbol{\theta}_{\rm cen}|\mathcal{D}^{\rm g}_{\rm obs}, \mathcal{R}_{\rm cen}) = \frac{\pi(\boldsymbol{\theta}_{\rm cen}|\mathcal{R}_{\rm cen})}{\pi(\mathcal{D}^{\rm g}_{\rm obs}|\mathcal{R}_{\rm cen})} \int_{\Omega(\mathcal{Z})} \int_{\Omega(\mathcal{D}^{\rm g}_{\rm int})} \pi(\mathcal{D}^{\rm g}_{\rm int}{}^{*}|\mathcal{D}^{\rm g}_{\rm obs}, \mathcal{Z}, \mathcal{R}_{\rm cen}, \boldsymbol{\theta}_{\rm cen}) \pi(\mathcal{Z}|\mathcal{R}_{\rm cen}, \boldsymbol{\theta}_{\rm cen}) \times d\mathcal{D}^{\rm g}_{\rm int}{}^{*}\, d\mathcal{Z}, \quad (18)$$

$$\overset{\text{i.i.d.}}{\propto} \exp\left(-\int_{\Omega(\boldsymbol{D}_{\rm int})} \mathcal{R}_{\rm cen}(\boldsymbol{D}^{*}_{\rm int}, \boldsymbol{\theta}_{\rm cen}) d\boldsymbol{D}^{*}_{\rm int}\right) \times \prod_{i=1}^{1366} \eta_{\rm eff}(\widehat{\boldsymbol{D}}^{\rm g}_{\rm obs,i}, \boldsymbol{\theta}_{\rm eff}) \int_{\Omega(\boldsymbol{D}_{\rm int})} \mathcal{R}_{\rm tru}(\boldsymbol{D}^{*}_{\rm int}, \boldsymbol{\theta}_{\rm tru}) \times \pi(\boldsymbol{D}^{*}_{\rm int} \mid \boldsymbol{D}^{\rm g}_{\rm obs,i}) d\boldsymbol{D}^{*}_{\rm int}, \quad (19)$$

$$\overset{\text{no noise}}{\equiv} \exp\left(-\int_{\Omega(\boldsymbol{D}_{\rm int})} \mathcal{R}_{\rm cen}(\boldsymbol{D}^{*}_{\rm int}, \boldsymbol{\theta}_{\rm cen}) d\boldsymbol{D}^{*}_{\rm int}\right) \times \prod_{i=1}^{1366} \eta_{\rm eff}(\widehat{\boldsymbol{D}}^{\rm g}_{\rm obs,i}, \boldsymbol{\theta}_{\rm eff}) \int_{z^{*}=0}^{z^{*}=+\infty} \mathcal{R}_{\rm tru}(\widehat{\boldsymbol{D}}^{\rm g}_{\rm obs,i}, z^{*}, \boldsymbol{\theta}_{\rm tru}) dz^{*}, \quad (20)$$

where Equation (19) holds under the assumption of an independent and identical distribution (i.e., the i.i.d. property) of BATSE LGRBs, and the second integration within it is performed over all possible realizations of the truth for the ith observed BATSE LGRB, $\boldsymbol{D}^{\rm g}_{\rm obs,i}$. Equation (19) can be further considerably simplified to Equation (20) by assuming no measurement uncertainty in the observational data, except redshift (z), which is completely unknown for BATSE LGRBs.

Once the posterior PDF of the model parameters is obtained, it can be plugged into Equation (16) to constrain the redshift PDF of individual BATSE LGRBs at the second level of modeling.

2.4. The LGRB Redshift Prior Knowledge

Our main assumption in this work is that the intrinsic comoving rate density of LGRBs closely traces the comoving SFR density (e.g., Madau & Dickinson 2014; Madau & Fragos 2017; Fermi-LAT Collaboration et al. 2018; hereafter M14, M17, F18, respectively) or a metallicity-corrected SFR density as prescribed by B10. Consequently, regardless of the individually unknown redshifts of BATSE LGRBs, the overall redshift distribution of all BATSE LGRBs together is enforced in our modeling to follow the cosmic SFR convolved with the BATSE detection efficiency model, $\eta_{\rm eff}$, which is detailed in Section 2.6. This assumption is essential for the success of our modeling approach, as any attempts to constrain the comoving rate density, $\dot{\zeta}(z)$, of LGRBs solely based on BATSE data leads to highly degenerate parameter space, $\Omega(\boldsymbol{\theta}_{\rm cen})$, and parameter estimates for our model, $\mathcal{R}_{\rm cen}$.

As for the choice of the LGRB rate density model, $\dot{\zeta}$, we have considered and simulated six different LGRB rate density scenarios, three of which have the generic continuous piecewise form,

$$\dot{\zeta}(z) \propto \begin{cases} (1+z)^{\gamma_0} & z < z_0 \\ (1+z)^{\gamma_1} & z_0 < z < z_1 \\ (1+z)^{\gamma_2} & z > z_1, \end{cases} \quad (21)$$

with parameters

$$\boldsymbol{\theta}_z = (z_0, z_1, \gamma_0, \gamma_1, \gamma_2) = \begin{cases} (0.97, 4.5, 3.4, -0.3, -7.8) & \text{(H06)} \\ (0.993, 3.8, 3.3, 0.055, -4.46) & \text{(L08)} \\ (0.97, 4.00, 3.14, 1.36, -2.92) & \text{(B10)} \\ (0.0, 4.5, 0.0, 0.0, -7.8) & \text{(P15)} \end{cases} \quad (22)$$

corresponding to the SFR density of Hopkins & Beacom (2006, hereafter H06), Li (2008, hereafter L08), and Petrosian et al. (2015, hereafter P15), and a bias-corrected redshift distribution of LGRBs derived from Swift data by B10. The other three redshift scenarios follow the generic functional of Equation

(15) in Madau & Dickinson (2014),

$$\dot{\zeta}(z) \propto \frac{(1+z)^{\alpha_1}}{(1+z)^{\alpha_2} + (1+z_0)^{\alpha_2}}, \tag{23}$$

with parameters

$$\boldsymbol{\theta}_z = (z_0,\, \alpha_1,\, \alpha_2) = \begin{cases} (1.90,\, 2.70,\, 5.60) & \text{(M14)} \\ (2.20,\, 2.60,\, 6.20) & \text{(M17).} \\ (1.63,\, 2.99,\, 6.19) & \text{(F18)} \end{cases} \tag{24}$$

For the sake of brevity, we will only present the results for four out of these seven SFR density scenarios: H06, B10, P15, M17.

2.5. The LGRB Property Rate Model: $\mathcal{R}^{\rm g}_{\rm tru}$

We model the joint four-dimensional distribution of $\boldsymbol{D}^{\rm g}_{\rm int}$ with a multivariate log-normal distribution, $\mathcal{R}^{\rm g}_{\rm tru} \equiv \mathcal{LN}$, whose parameters (i.e., the mean vector and the covariance matrix), $\boldsymbol{\theta}^{\rm g}_{\rm tru} = \{\boldsymbol{\mu}, \boldsymbol{\Sigma}\}$, will have to be constrained by data. The justification for the choice of a multivariate log-normal as the underlying intrinsic population distribution of LGRBs is multifold. First, the observed joint distribution of BATSE LGRB properties highly resembles a log-normal shape that is censored close to the detection threshold of BATSE. Second, unlike the power-law distribution which has traditionally been the default choice of model for the luminosity function of LGRBs, log-normal models provide natural upper and lower bounds on the total energy budget and luminosity of LGRBs, eliminating the need for setting artificially sharp bounds on the distributions to properly normalize them. Third, a log-normal along with a Gaussian distribution is among the most naturally occurring statistical distributions in nature, whose generalizations to multiple dimensions are also well studied and understood. This is a highly desired property especially for our work, given the overall mathematical and computational complexity of the model proposed and developed here.

2.6. The BATSE Trigger Efficiency: $\eta_{\rm eff}$

Compared to the Fermi Gamma-ray Burst Monitor (Meegan et al. 2009) and Neil Gehrels Swift Observatory (Gehrels et al. 2004; Lien et al. 2016), BATSE had a relatively simple triggering algorithm. The BATSE detection efficiency and algorithm has been already extensively studied by the BATSE team as well as independent authors (e.g., Pendleton et al. 1998, 1995; Hakkila et al. 2003; see Shahmoradi & Nemiroff 2010, 2011a; Shahmoradi 2013a; Shahmoradi & Nemiroff 2015 for further discussion and references). However, simple implementation and usage of the known BATSE trigger threshold for modeling the BATSE catalog's sample incompleteness can lead to systematic biases in the inferred quantities of interest. BATSE triggered on 2702 GRBs, out of which only 2145, or approximately 79%, have been consistently analyzed and reported in the current BATSE catalog, with the remaining 21% either having a low accumulation of count rates or missing full spectral/temporal coverage (Goldstein et al. 2013). Thus, the extent of sample incompleteness in the BATSE catalog is likely not fully and accurately represented by the BATSE triggering algorithm alone.

BATSE LADs generally triggered on a GRB if the number of photons per 1024 [ms] arriving at the detectors in the 50–300 [keV] energy window, $P_{\rm ph}$, reached a certain threshold in units of the background photon count fluctuations, σ. This threshold

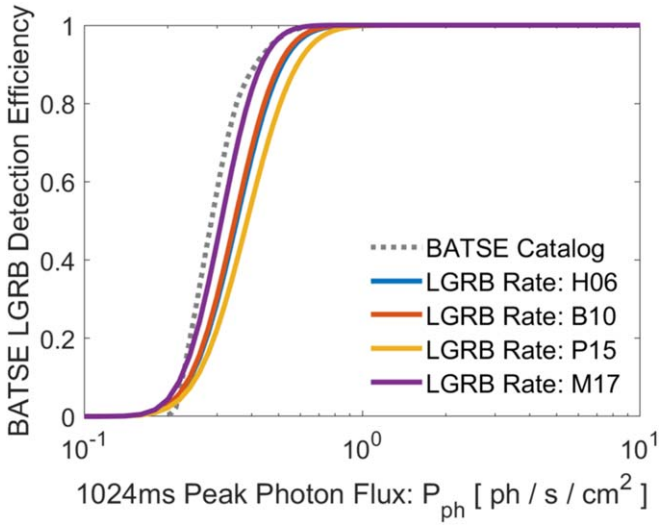

Figure 3. Comparison of the BATSE 4B Catalog nominal LGRB-detection efficiency as a function of the 1024 [ms] peak photon flux, $P_{\rm ph}$, with the predicted detection efficiencies in this work based on the four different LGRB rate models considered: H06, B10, P15, M17. The peak photon flux, $P_{\rm ph}$, is measured in the BATSE energy window 50–300 [keV].

was typically set to 5.5σ during much of BATSE's operational lifetime. However, the naturally occurring fluctuations in the average background photon counts effectively lead to a monotonically increasing BATSE detection efficiency as a function of $P_{\rm ph}$ instead of a sharp cutoff on the observed $P_{\rm ph}$ distribution of LGRBs. Therefore, we model the effects of BATSE detection efficiency and sample incompleteness more accurately by an error function,

$$\pi(\text{detection}|\mu_{\rm th},\, \sigma_{\rm th},\, P_{\rm ph}) = \frac{1}{2} + \frac{1}{2} \times \text{erf}\left(\frac{\log_{10} P_{\rm ph} - \mu_{\rm th}}{\sigma_{\rm th}\sqrt{2}}\right), \tag{25}$$

that, for a given set of the error function's parameters ($\boldsymbol{\theta}_{\rm eff} = \{\mu_{\rm th},\, \sigma_{\rm th}\}$), yields the probability of the detection of an LGRB with $P_{\rm ph}$ photon counts per second. Due to the unknown effects of sample incompleteness on BATSE data, we leave these two threshold parameters free solely to be constrained by the observational data. Figure 3 compares the resulting best-fit detection efficiency functions for BATSE under different SFR scenarios with the BATSE nominal detection efficiency for LGRBs[4] (see also Pendleton et al. 1995, 1998; Paciesas et al. 1999; Hakkila et al. 2003; Shahmoradi 2013a; Shahmoradi & Nemiroff 2015).

The current BATSE catalog already provides estimates of $P_{\rm ph}$ for all 1366 LGRBs in our analysis. The connection between $P_{\rm ph}$ and the bolometric 1024 [ms] peak flux, $P_{\rm bol}$, which is used in our modeling, is provided by fitting all LGRB spectra with a smoothly broken power law,

$$\Phi(E) \propto \begin{cases} E^{\alpha} \mathrm{e}^{\left(-\frac{(1+z)(2+\alpha)E}{E_{\rm pz}}\right)} & \text{if } E \leqslant \left(\frac{E_{\rm pz}}{1+z}\right)\left(\frac{\alpha-\beta}{2+\alpha}\right), \\ E^{\beta} & \text{if otherwise} \end{cases} \tag{26}$$

[4] Available at https://gammaray.nsstc.nasa.gov/batse/grb/catalog/4b/4br_efficiency.html.

Table 1
Mean Best-fit Parameters of the LGRB World Model, Equation (10), for the Four Redshift Distribution Scenarios Considered

Parameter	H06	B10	P15	M17
Location Parameters($\boldsymbol{\mu}$)				
$\mu_{\log_{10}(L_{\rm iso})}$	51.40 ± 0.24	51.95 ± 0.16	50.91 ± 0.22	52.01 ± 0.08
$\mu_{\log_{10}(E_{\rm pz})}$	2.43 ± 0.06	2.59 ± 0.05	2.31 ± 0.06	2.59 ± 0.02
$\mu_{\log_{10}(E_{\rm iso})}$	51.86 ± 0.25	52.24 ± 0.18	51.38 ± 0.23	52.46 ± 0.09
$\mu_{\log_{10}(T_{90z})}$	1.13 ± 0.03	1.00 ± 0.04	1.10 ± 0.05	1.15 ± 0.02
Scale Parameters (Diagonal Elements of $\boldsymbol{\Sigma}$)				
$\sigma_{\log_{10}(L_{\rm iso})}$	0.59 ± 0.10	0.56 ± 0.06	0.58 ± 0.09	0.33 ± 0.05
$\sigma_{\log_{10}(E_{\rm pz})}$	0.37 ± 0.02	0.36 ± 0.02	0.38 ± 0.02	0.34 ± 0.01
$\sigma_{\log_{10}(E_{\rm iso})}$	0.85 ± 0.08	0.87 ± 0.06	0.88 ± 0.08	0.67 ± 0.04
$\sigma_{\log_{10}(T_{90z})}$	0.43 ± 0.01	0.42 ± 0.01	0.43 ± 0.01	0.43 ± 0.01
Correlation Coefficients (Nondiagonal Elements of $\boldsymbol{\Sigma}$)				
$\rho_{L_{\rm iso}-E_{\rm pz}}$	0.49 ± 0.07	0.42 ± 0.08	0.56 ± 0.08	0.34 ± 0.08
$\rho_{L_{\rm iso}-E_{\rm iso}}$	0.93 ± 0.01	0.97 ± 0.01	0.97 ± 0.01	0.95 ± 0.02
$\rho_{L_{\rm iso}-T_{90z}}$	0.46 ± 0.09	0.66 ± 0.06	0.67 ± 0.09	0.65 ± 0.08
$\rho_{E_{\rm pz}-E_{\rm iso}}$	0.60 ± 0.04	0.58 ± 0.04	0.61 ± 0.05	0.51 ± 0.04
$\rho_{E_{\rm pz}-T_{90z}}$	0.30 ± 0.04	0.42 ± 0.04	0.34 ± 0.04	0.30 ± 0.03
$\rho_{E_{\rm iso}-T_{90z}}$	0.59 ± 0.05	0.68 ± 0.04	0.69 ± 0.05	0.67 ± 0.03
BATSE Detection Efficiency (Sample Incompleteness)				
μ_{rmth}	−0.45 ± 0.02	−0.46 ± 0.02	−0.41 ± 0.02	−0.51 ± 0.02
$\sigma_{\rm th}$	0.13 ± 0.01	0.13 ± 0.01	0.14 ± 0.01	0.11 ± 0.02

known as the Band model (Band et al. 1993) to infer their spectral normalization constants while fixing the low- and high-energy photon indices of the Band model to the corresponding population averages $(\alpha, \beta) = (-1.1, -2.3)$ and fixing the observed spectral peak energies, $E_{\rm p}$, of individual bursts to the corresponding best-fit values from Shahmoradi & Nemiroff (2010). Such an approximation is reasonable given the typically large uncertainties that exist in the spectral and temporal properties of GRBs (e.g., Butler et al. 2010; Shahmoradi 2013a) and the relatively large variance of the population distribution of $P_{\rm bol}$ in our sample.

3. Results

We proceed by first fitting the proposed censored cosmic LGRB rate model, $\mathcal{R}_{\rm cen}$, to 1366 BATSE LGRB data under the six LGRB redshift distribution scenarios prescribed by Equations (21)–(22) and Equations (23)–(24). For each LGRB rate density scenario, the posterior PDF of parameters in Equation (19) is explored by a Parallel Delayed-Rejection Adaptive Metropolis-Hastings Markov Chain Monte Carlo algorithm (the ParaDRAM algorithm) that we have developed for such sampling tasks as part of a larger Monte Carlo simulation package named ParaMonte available in the C/C++/Fortran/MATLAB/Python programming languages[5] (e.g., Kumbhare & Shahmoradi 2020; Shahmoradi et al. 2020; Shahmoradi & Bagheri 2020a, 2020b).

The computations for each SFR scenario are performed on 96 processors in parallel on two Skylake compute-nodes of the Stampede2 supercomputer at the Texas Advanced Computing Center. We ran extensive tests to ensure a high-level of accuracy of the high-dimensional numerical integrations involved in the derivation of the posterior distribution of the parameters of the censored cosmic rate model for LGRBs as given in Equation (18). For the sake of brevity, the resulting best-fit parameters corresponding to only four out of these six SFR densities are tabulated in Table 1, and the marginal distributions of their parameters are compared with each other in Figure 4.

Once the parameters of the censored cosmic rate model Equation (11) are constrained, we use the calibrated model at the second level of our analysis to further constrain the PDFs of the unknown redshifts of individual BATSE LGRBs according to Equation (16). Similar to the Empirical Bayes methodology, this iterative process can continue until convergence to a specific set of redshift PDFs occurs. However, given the computational complexity and the expense of each iteration, we stop after obtaining the first round of estimates. This is also a common practice in the Empirical Bayes modeling. To further reduce the computational complexities of the simulations, we also drop the measurement uncertainties described by Equation (1) in all observational data from both levels of the analysis in Equations (19) and (16). To further reduce the computational expense of the inference, we also approximate the numerical integration in the definition of the luminosity distance in Equation (6) by the analytical expressions of Wickramasinghe & Ukwatta (2010). All routines were implemented in the Fortran programming language and comply with the latest Fortran Standard published in 2018 (e.g.,

[5] Available at https://github.com/cdslaborg/paramonte.

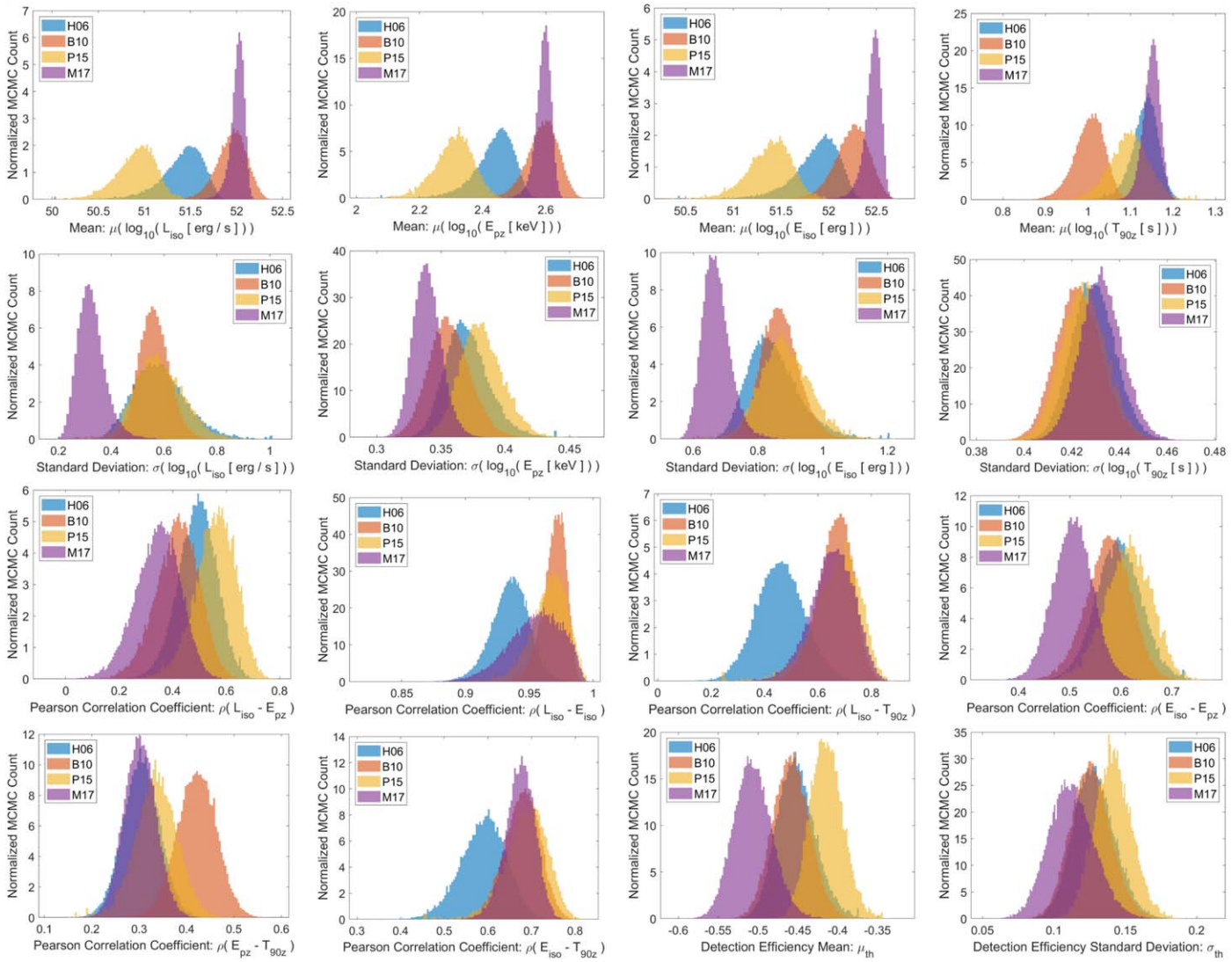

Figure 4. Marginal posterior distributions of the 16 parameters of the LGRB world model, for the four redshift distributions considered in this work, H06, B10, P15, M17, as given by Equations (21), (22), (23), and (24).

Table 2
BATSE 1366 LGRB Redshift Estimates

Trigger	$\mu_{Z,H06}$	$PI_{90\%}$	$\mu_{Z,B10}$	$PI_{90\%}$	$\mu_{Z,M17}$	$PI_{90\%}$	$\mu_{Z,P15}$	$PI_{90\%}$
105	0.46	[0.22, 0.81]	0.59	[0.39, 0.83]	0.56	[0.43, 0.71]	0.49	[0.37, 0.60]
107	1.61	[0.88, 2.56]	2.70	[1.98, 3.55]	2.55	[1.92, 3.15]	2.30	[1.68, 2.81]
109	1.69	[0.93, 2.71]	3.24	[2.53, 4.02]	1.90	[1.57, 2.31]	1.59	[1.32, 1.90]
110	2.48	[1.31, 3.87]	4.47	[3.53, 5.57]	3.33	[2.61, 3.98]	2.93	[2.24, 3.47]
111	2.46	[1.29, 3.87]	4.62	[3.67, 5.75]	3.09	[2.50, 3.67]	2.61	[2.08, 3.06]

Note. The column denoted by "Trigger" contains the trigger IDs of BATSE LGRBs. The columns denoted by μ_{H06}, μ_{B10}, μ_{M17}, and μ_{F18} contain the predicted mean redshifts of the individual BATSE LGRBs, based on the four LGRB rate model assumptions (H06, B10, M17, F18) considered in this work as given by Equations (21), (22), (23), and (24). The rest of the columns denoted by "$PI_{90\%}$" contain the lower and upper bounds of the 90% prediction intervals (i.e., the most probable ranges) for the unknown redshifts of individual BATSE LGRBs. This table as well as the full probability density functions of the redshifts of individual BATSE LGRBs in available for download at the permanent GitHub repository of this work. Table 2 is published in its entirety in machine-readable format. A portion is shown here for guidance regarding its form and content.

(This table is available in its entirety in machine-readable form.)

Metcalf et al. 2011, 2018; Reid 2018).[6] The complete set of 1366 BATSE LGRBs observational data is also publicly available for download at the project's permanent repository on GitHub. The mean redshifts together with the 90% prediction intervals for the four LGRB rate density scenarios are also reported in Table 2. We find that, on average, the redshifts of individual BATSE LGRBs can be constrained to within 50% uncertainty ranges of 0.55, 0.46, 0.32, and 0.25, corresponding

[6] Available at https://github.com/cdslaborg/BatseLgrbRedshiftCatalog.

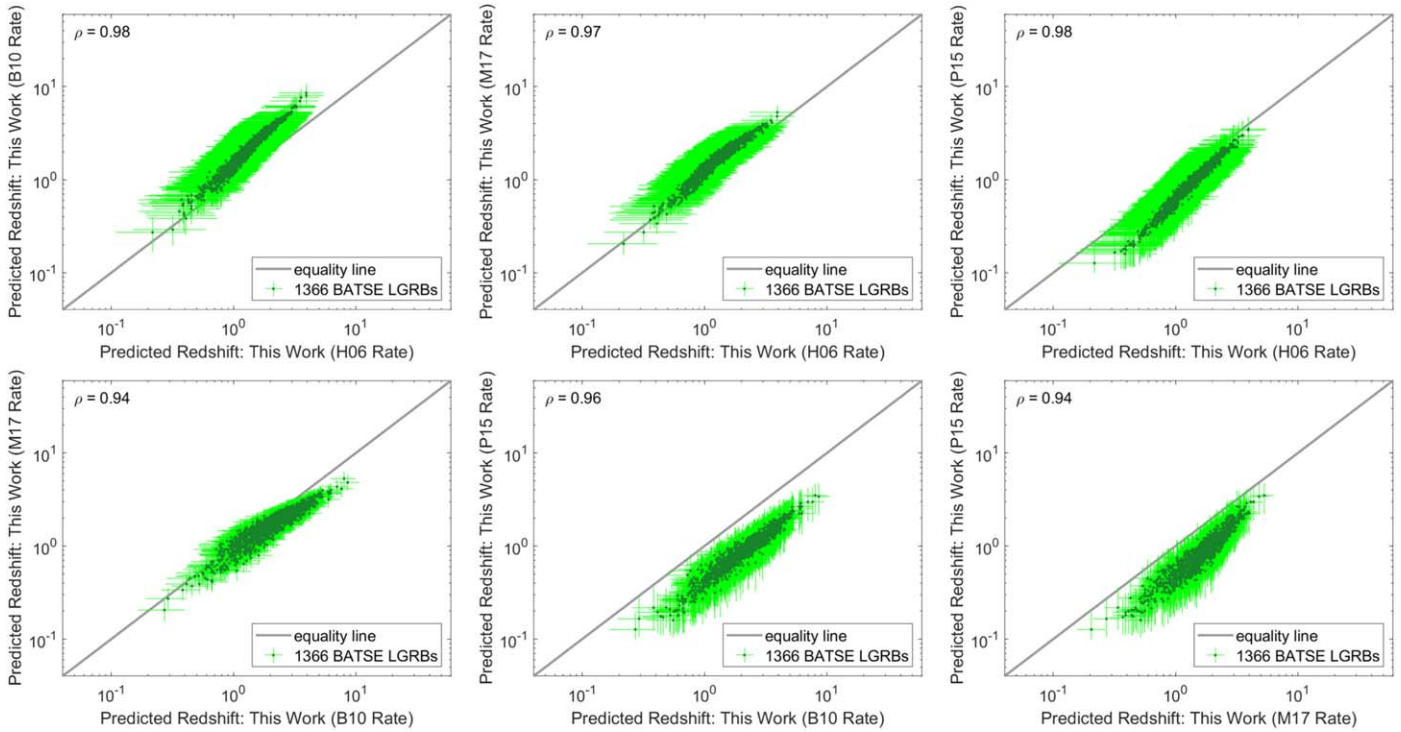

Figure 5. Comparison of the expected redshifts of 1366 BATSE LGRBs for the four different cosmic LGRB rate density assumptions, Equation (21), with each other. In each plot, the Spearman's correlation coefficient of the two sets of expected redshifts is also reported. The error bars represent the 90% prediction intervals of each individual redshift.

to the four LGRB rate densities of H06, B10, P15, and M17, respectively. At the 90% confidence level, the prediction intervals expand to wider uncertainty ranges of 1.40, 1.15, 0.82, and 0.71, respectively.

4. Discussion

In this work, we proposed a semi-Bayesian methodology to infer the unknown redshifts of 1366 BATSE catalog LGRBs. Toward this, first, we segregated the two populations of BATSE LGRBs and SGRBs using the fuzzy C-means classification method based on the observed duration and spectral peak energies of 1966 BATSE GRBs with available spectral and temporal information. We then modeled the process of LGRB detection as a nonhomogeneous spatiotemporal Poisson process, whose rate parameter is modeled by a multivariate log-normal distribution as a function of the four main LGRB intrinsic attributes: the 1024 [ms] isotropic peak luminosity ($L_{\rm iso}$), the total isotropic emission ($E_{\rm iso}$), the intrinsic spectral peak energy ($E_{\rm pz}$), and the intrinsic duration (T_{90z}). We stress again that due to our limited knowledge of the BATSE LGRB redshifts, this assumption is necessary to infer the redshifts. To calibrate the parameters of the rate model, we made the fundamental assumption that LGRBs trace the cosmic SFR or a metallicity-corrected SFR. For each of the individual LGRB rate densities considered in this work, H06, B10, P15, M17, we then used the resulting posterior probability densities of the model parameters to compute the probability density functions of the redshifts of individual BATSE LGRBs.

As illustrated in Figure 5, we find that the individual redshift estimates of BATSE LGRBs for the LGRB rate density assumptions are broadly consistent with each other. There are, however, systematic differences between the estimates, the most significant of which is the difference between the expected redshifts based on B10 and the other rate densities. The difference can be explained by the larger rates of LGRBs that the model of B10 implies at higher redshifts compared to the other rate scenarios that exactly model the SFR in the universe. This, in effect, shifts the expected redshifts of BATSE LGRBs systematically toward larger values.

As we explained in Section 2.2, the underlying logic of our approach to resolving the individual redshifts of BATSE LGRBs can be qualitatively understood by reconsidering the set of Equations (4). Taking the logarithm of both sides of all equations, we obtain a set of linear maps from the rest-frame to the observer-frame properties of LGRBs, Equation (7). Therefore, the distributions of the four observer-frame LGRB properties result from the convolution of the distributions of the corresponding rest-frame LGRB properties with the distribution of terms that are exactly determined by redshift (i.e., the logarithm of the luminosity distance $\log_{10}(d_L)$ and the term $\log_{10}(z+1)$).

The larger the variances of the redshift-related terms in these equations (compared to the variances of rest-frame LGRB attributes), the more the observer-frame LGRB properties will be indicative of the redshifts of individual events. For example, the LGRB rate density of M17 results in the largest ratios of the variances of redshift-related terms, Equation (4), to the variances of the intrinsic BATSE LGRB attributes. This, in turn, leads to the least uncertain (but not necessarily the most accurate) individual redshift predictions under the rate density assumptions of M17 among all rate densities considered in this study. This is also evidenced in the plots of Figures 5 and 6 by the relatively tighter prediction intervals (i.e., error bars) for the redshift estimates based on the LGRB rate density of M17.

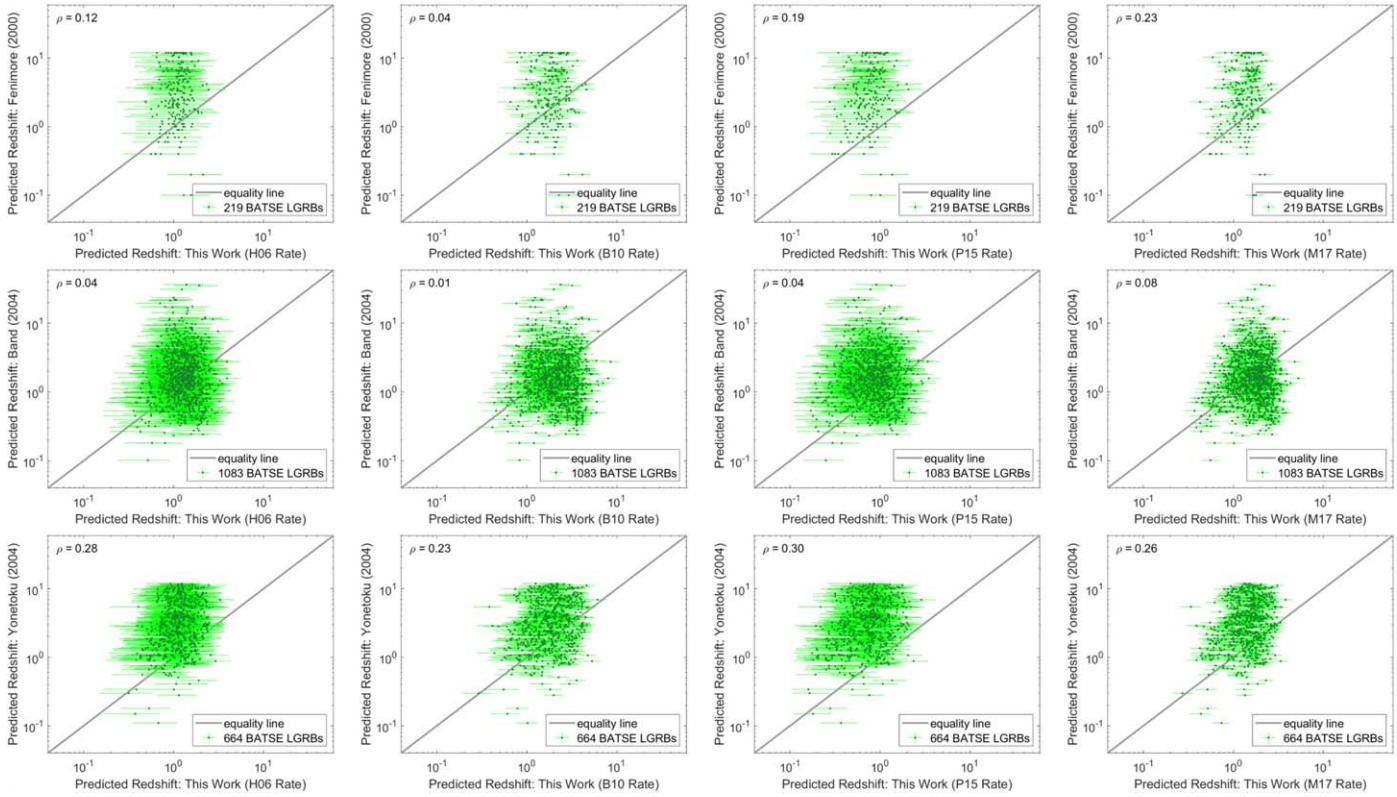

Figure 6. Comparison of the expected redshifts of BATSE LGRBs under the four different cosmic LGRB rate density assumptions, Equation (21), with the BATSE redshift estimates from previous works, based on the correlation between lightcurve variability and peak luminosity by Fenimore & Ramirez-Ruiz (2000), the lag-luminosity relation by Band et al. (2004), and the correlation between the peak luminosity and the spectral peak energy by Yonetoku et al. (2004). On each plot, the Spearman's correlation coefficient of the two sets of expected redshifts is also reported. The error bars represent the 90% prediction intervals for each predicted redshift in this work.

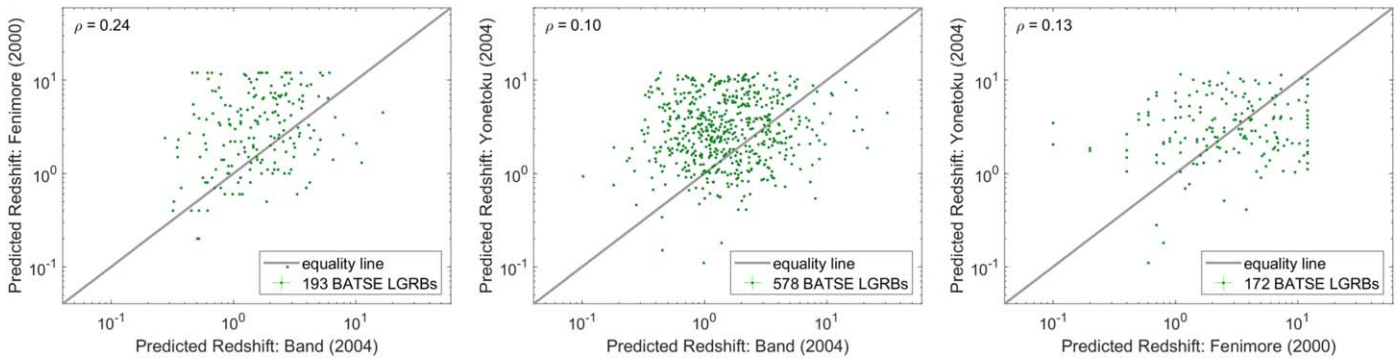

Figure 7. Comparison of the predicted redshifts of BATSE GRBs with each other based on the correlation between lightcurve variability and peak luminosity by Fenimore & Ramirez-Ruiz (2000), the lag-luminosity relation by Band et al. (2004), and the correlation between the peak luminosity and the spectral peak energy by Yonetoku et al. (2004). On each plot, the Pearson's correlation coefficient of the two sets of predicted redshifts is also reported.

Several previous studies have attempted to estimate the unknown redshifts of BATSE LGRBs via some of the phenomenological gamma-ray correlations. For example, Fenimore & Ramirez-Ruiz (2000) used the apparent correlation between the isotropic peak luminosity of GRBs and the temporal variability of their lightcurves to estimate the redshifts of 220 BATSE GRBs. Band et al. (2004) used the apparent correlation between the spectral lag and the peak luminosity of GRBs to estimate the unknown redshifts of 1194 BATSE events. Similarly, Yonetoku et al. (2004) used the apparent observed correlation between the isotropic peak luminosity and the intrinsic spectral peak energies of GRBs to estimate the redshifts of 689 BATSE GRBs.

We compare our redshift estimates under different LGRB rate density assumptions to the predictions of each of the aforementioned works in Figure 6. None of these three previous independent redshift estimates based on the high-energy correlations appear to agree with our predictions. These three independent estimates are also highly inconsistent with each other as shown in Figure 7.

The observed inconsistencies of the previous independent redshift estimates of BATSE GRBs with each other, as well as with the predictions of this work, may be explained by the fact that the prompt gamma-ray correlations used in the works of Fenimore & Ramirez-Ruiz (2000), Band et al. (2004), and Yonetoku et al. (2004) were constructed from a small sample of

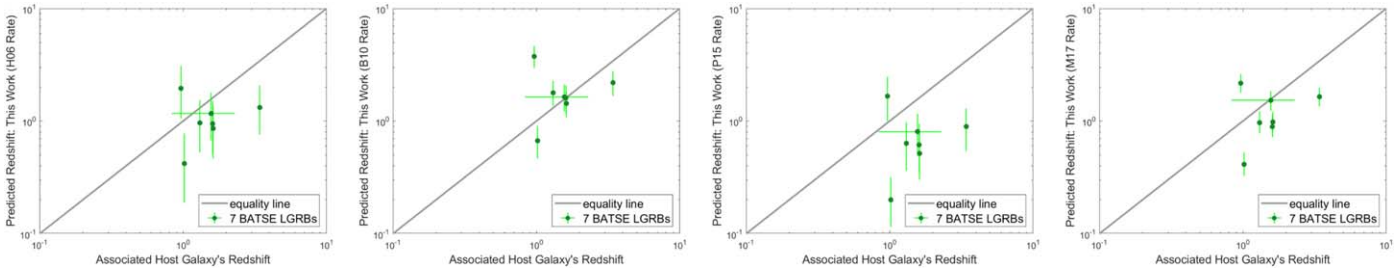

Figure 8. Comparison of the predicted redshifts of a set of BATSE LGRBs with their reported measured redshifts in the literature, for the four LGRB rate density assumptions of H06, B10, P15, and M17. The error bars represent the 90% uncertainty intervals for the predicted redshifts and the 100% uncertainty intervals for the measured redshifts (where available).

heterogeneously collected GRB events, and that the observed phenomenological relations are likely severely affected by sample incompleteness. Despite the discrepancies in the redshift estimates of individual BATSE LGRBs, our predictions corroborate the findings of some previous studies (e.g., Ashcraft & Schaefer 2007; Hakkila et al. 2009) in that the probability of the existence of very high-redshift LGRBs in the BATSE catalog is negligible.

As illustrated in Figure 6, the fact that the redshift estimates of Yonetoku et al. (2004) show the least disagreement with our predictions among all previous attempts can be explained by noting the relative similarity of the assumptions in Yonetoku et al. (2004) to infer the redshifts with the findings of this work: Yonetoku et al. (2004) inferred the redshifts based on the assumption of the existence of a tight positive correlation between the intrinsic spectral peak energy and the peak luminosity of LGRBs. Our modeling approach confirms the existence of such a positive correlation (see Table 1), albeit with a much higher dispersion and lower strength. The disparity in the predicted strength and regression slope of this correlation can reasonably explain the non-negligible disagreement between our predictions and those of Yonetoku et al. (2004).

Finally, we compare our predictions with the measured redshifts of BATSE events, where available. Out of 2702 BATSE LGRBs, only fewer than a dozen have measured redshifts through association with their potential host galaxies. In Figure 8, we compare the reported redshifts of seven such BATSE events (that also exist in our catalog) with their corresponding predicted redshifts in this work. Among all LGRB rate density models considered, the predicted redshifts based on the LGRB rate of B10 appear to show the highest level of consistency with the measured redshifts. This leads us to cautiously conclude that the LGRB formation rate may not exactly trace the star formation rate in the distant universe, corroborating the previous finding of B10, Shahmoradi (2013a), and Shahmoradi & Nemiroff (2015).

While being a remote possibility, one of the potential caveats of our presented redshift estimates is that, if an SGRB has been mistakenly classified as an LGRB in our catalog of 1366 by our classification method described in Section 2.1, then its estimated redshift may not be accurate. Also, this work did not take into account the potential effects of the GRBs' jet-beaming angle. A recent study by Lazzati et al. (2013) finds that the different orientations of the GRB jet axis with respect to the observer could partially explain the observed LGRB brightness–hardness type relations. Such an effect could potentially lead to more uncertainty in the predicted redshifts and perhaps could explain the lack of a complete perfect agreement between the known redshifts of a handful of BATSE LGRBs and their corresponding predicted redshifts in this work, as illustrated by the plots of Figure 8. These are among the improvements that could be made in the future to our mathematically rigorous, purely probabilistic, bias-aware approach to estimating or further constraining the unknown redshifts of GRBs in currently available and future GRB catalogs.

4.1. The Redshift Dependence of the Luminosity Function and the Excess Rate of LGRBs at Low Redshifts

A remarkable modeling assumption in our work is the redshift independence of the proposed model for the four main gamma-ray properties of cosmic LGRBs (the term $\mathcal{R}^{\rm g}_{\rm tru}$ in Equation (12)). This modeling assumption is similar to the assumptions of Shahmoradi (2013a) and Shahmoradi & Nemiroff (2015) and follows the findings of B10, who, based on a multivariate analysis of a large sample of Swift LGRBs with and without redshifts, reject the hypothesis of an evolving redshift-dependent luminosity function for LGRBs. This is in contrast to the findings of Petrosian et al. (2015), Yu et al. (2015), Pescalli et al. (2016), Tsvetkova et al. (2017), and Lloyd-Ronning et al. (2019), who model the cosmic rates of LGRBs via a redshift-dependent luminosity function.

Regardless of the validity of the aforementioned assumption in our modeling, we note that it is practically impossible to infer any redshift dependence of the energetics and the luminosity function of LGRBs solely via BATSE LGRB data. This limitation primarily results from the complete lack of knowledge of the redshifts of BATSE LGRBs. This missing knowledge leads to a highly degenerate parameter space for models that consider the possibility of a redshift evolution of the prompt emission properties of LGRBs.

The multivariate log-normal luminosity function assumption of this work also needs to be further studied and validated, and its effects on the inferred redshifts understood better in a future work. As illustrated in Figure 2, the accuracy of the inferred redshifts of LGRBs depends strongly on the width of the redshift distribution relative to the intrinsic distributions of LGRB properties, most importantly, the $L_{\rm iso}$ and $E_{\rm iso}$ distributions. If the intrinsic LGRB property distributions are too broad compared with the redshift distribution, then one would expect less accurate redshift estimates. However, we anticipate that the particular choice of the luminosity function (for example, log-normal versus power law or broken power law) will have minimal effects on the inferred redshifts because the detection threshold of gamma-ray telescopes cuts the intrinsic LGRB property distributions before any noticeable statistically significant discrepancies between the different choices of

energetics distributions could be identified solely from the observational data. This is an important issue that needs further investigation and validation in the future.

The investigation of the evidence for the luminosity evolution of LGRBs goes beyond the scope of this manuscript. We instead defer a detailed investigation of this problem to a future paper. Nevertheless, we emphasize that the results presented in this manuscript are completely based on the validity of the assumption of the redshift independence of the luminosity function of LGRBs (e.g., Butler et al. 2010) that has been recently challenged by independent studies (e.g., Petrosian et al. 2015; Yu et al. 2015; Pescalli et al. 2016; Tsvetkova et al. 2017; Lloyd-Ronning et al. 2019).

We thank the anonymous referee of this manuscript whose criticisms and comments significantly improved the quality and accuracy of the conclusions of this paper. This work would have not been accomplished without the vast time and effort spent by many scientists and engineers who designed, built, and launched the Compton Gamma-ray Observatory and were involved in the analysis of GRB data from BATSE Large Area Detectors.

ORCID iDs

Joshua A. Osborne https://orcid.org/0000-0003-1321-748X
Amir Shahmoradi https://orcid.org/0000-0002-9720-8937
Robert J. Nemiroff https://orcid.org/0000-0002-4505-6599

References

Ashcraft, T., & Schaefer, B. E. 2007, ApJ, 671, 1896
Band, D., Matteson, J., Ford, L., et al. 1993, ApJ, 413, 281
Band, D. L., Norris, J. P., & Bonnell, J. T. 2004, ApJ, 613, 484
Band, D. L., & Preece, R. D. 2005, ApJ, 627, 319
Bernardini, M. G., Ghirlanda, G., Campana, S., et al. 2014, MNRAS, 446, 1129
Butler, N. R., Bloom, J. S., & Poznanski, D. 2010, ApJ, 711, 495
Butler, N. R., Kocevski, D., & Bloom, J. S. 2009, ApJ, 694, 76
Butler, N. R., Kocevski, D., Bloom, J. S., & Curtis, J. L. 2007, ApJ, 671, 656
Dainotti, M., Petrosian, V., Bogdan, M., et al. 2019, arXiv:1907.05074
Dainotti, M. G., Del Vecchio, R., Shigehiro, N., & Capozziello, S. 2015, ApJ, 800, 31
Dempster, A. P., Laird, N. M., & Rubin, D. B. 1977, Journal of the Royal Statistical Society: Series B (Methodological), 38, 1
Fenimore, E., Norris, J., Bonnell, J., Nemiroff, R., et al. 1995, ApJL, 448, L101
Fenimore, E. E., & Ramirez-Ruiz, E. 2000, arXiv:astro-ph/0004176
Fermi-LAT Collaboration, Abdollahi, S., & Ackermann, M. 2018, Sci, 362, 1031
Gehrels, N., Ramirez-Ruiz, E., & Fox, D. B. 2009, ARA&A, 47, 567
Gehrels, N., Chincarini, G., Giommi, P., et al. 2004, ApJ, 611, 1005
Gehrels, N., Norris, J., Barthelmy, S., et al. 2006, Natur, 444, 1044
Ghirlanda, G., Nava, L., Ghisellini, G., Firmani, C., & Cabrera, J. 2008, MNRAS, 387, 319
Goldstein, A., Preece, R. D., Mallozzi, R. S., et al. 2013, ApJS, 208, 21
Goldstein, A., Preece, R. D., Briggs, M. S., et al. 2011, arXiv:1101.2458
Guidorzi, C. 2005, MNRAS, 364, 163
Hakkila, J., Fragile, P. C., & Giblin, T. W. 2009, in AIP Conf. Proc. 1133, Gamma-Ray Burst: Sixth Huntsville Symp., ed. C. A. Meegan, N. Gehrels, & C. Kouveliotou (Melville, NY: AIP), 479
Hakkila, J., Giblin, T. W., Roiger, R. J., et al. 2003, ApJ, 582, 320
Hopkins, A. M., & Beacom, J. F. 2006, ApJ, 651, 142
Jarosik, N., Bennett, C., Dunkley, J., et al. 2011, ApJS, 192, 14
Kouveliotou, C., Meegan, C. A., Fishman, G. J., et al. 1993, ApJL, 413, L101
Kumbhare, S., & Shahmoradi, A. 2020, arXiv:2010.04190
Lazzati, D., Morsony, B. J., Margutti, R., & Begelman, M. C. 2013, ApJ, 765, 103
Li, L.-X. 2008, MNRAS, 388, 1487
Lien, A., Sakamoto, T., Barthelmy, S. D., et al. 2016, ApJ, 829, 7
Lloyd, N. M., & Petrosian, V. 1999, ApJ, 511, 550
Lloyd, N. M., Petrosian, V., & Mallozzi, R. S. 2000, ApJ, 534, 227
Lloyd-Ronning, N. M., Aykutalp, A., & Johnson, J. L. 2019, MNRAS, 488, 5823
Lü, H.-J., Zhang, B., Liang, E.-W., Zhang, B.-B., & Sakamoto, T. 2014, MNRAS, 442, 1922
Madau, P., & Dickinson, M. 2014, ARA&A, 52, 415
Madau, P., & Fragos, T. 2017, ApJ, 840, 39
Meegan, C., Fishman, G., Wilson, R., et al. 1992, Natur, 355, 143
Meegan, C., Lichti, G., Bhat, P., et al. 2009, ApJ, 702, 791
Metcalf, M., Reid, J., & Cohen, M. 2011, Modern Fortran Explained (Oxford: Oxford Univ. Press)
Metcalf, M., Reid, J., & Cohen, M. 2018, Modern Fortran Explained: Incorporating Fortran (Oxford: Oxford Univ. Press)
Nakar, E., & Piran, T. 2004, MNRAS, 360, 73
Nava, L., Ghirlanda, G., Ghisellini, G., & Firmani, C. 2008, MNRAS, 391, 639
Nemiroff, R. J. 2000, ApJ, 544, 805
Paciesas, W. S., Meegan, C. A., Pendleton, G. N., et al. 1999, ApJS, 122, 465
Peebles, P. J. E. 1993, Principles of Physical Cosmology (Princeton, NJ: Princeton Univ. Press)
Pendleton, G., Hakkila, J., & Meegan, C. 1998, AIP Conf. Proc. 428, Fourth Huntsville Gamma-Ray Burst Symp. (Melville, NY: AIP), 899
Pendleton, G. N., Paciesas, W. S., Mallozzi, R. S., et al. 1995, NIMPA, 364, 567
Pescalli, A., Ghirlanda, G., Salvaterra, R., et al. 2016, A&A, 587, A40
Petrosian, V., Kitanidis, E., & Kocevski, D. 2015, ApJ, 806, 44
Petrosian, V., & Lee, T. T. 1996, ApJL, 467, L29
Petrosian, V., Lloyd-Ronning, N. M., & Lee, A. 1999, arXiv:astro-ph/9906393
Pontzen, A., Deason, A., Governato, F., et al. 2010, MNRAS, 402, 1523
Qin, Y., Liang, E.-W., Liang, Y.-F., et al. 2012, ApJ, 763, 15
Qin, Y.-P., & Chen, Z.-F. 2013, MNRAS, 430, 163
Reichart, D. E., Lamb, D. Q., Fenimore, E. E., et al. 2001, ApJ, 552, 57
Reid, J. 2018, ACM SIGPLAN Fortran Forum, 5, doi:10.1145/3206214.3206215
Rizzuto, D., Guidorzi, C., Romano, P., et al. 2007, MNRAS, 379, 619
Robbins, H. 1985, Herbert Robbins Selected Papers (Berlin: Springer), 41
Schaefer, B. E., Deng, M., & Band, D. L. 2001, ApJL, 563, L123
Shahmoradi, A. 2013a, ApJ, 766, 111
Shahmoradi, A. 2013b, arXiv:1308.1097
Shahmoradi, A. 2017, arXiv:1711.10599
Shahmoradi, A., & Bagheri, F. 2020a, arXiv:2008.09589
Shahmoradi, A., & Bagheri, F. 2020b, arXiv:2009.14229
Shahmoradi, A., Bagheri, F., & Osborne, J. A. 2020, arXiv:2010.00724
Shahmoradi, A., & Nemiroff, R. 2009, AIP Conf. Proc. 1133, Gamma-Ray Burst: Sixth Huntsville Symp. (Melville, NY: AIP), 425
Shahmoradi, A., & Nemiroff, R. 2011a, MNRAS, 411, 1843
Shahmoradi, A., & Nemiroff, R. 2011b, AAS Meeting 217, 249.05
Shahmoradi, A., & Nemiroff, R. 2014, AAS Meeting 223, 223, 330.03
Shahmoradi, A., & Nemiroff, R. J. 2010, MNRAS, 407, 2075
Shahmoradi, A., & Nemiroff, R. J. 2015, MNRAS, 451, 126
Tsvetkova, A., Frederiks, D., Golenetskii, S., et al. 2017, ApJ, 850, 161
Wickramasinghe, T., & Ukwatta, T. 2010, MNRAS, 406, 548
Winberg, S. (ed.) 1972, Gravitation and Cosmology: Principles and Applications of the General Theory of Relativity (New York: Wiley)
Xiao, L., & Schaefer, B. E. 2009, ApJ, 707, 387
Yonetoku, D., Murakami, T., Nakamura, T., et al. 2004, ApJ, 609, 935
Yonetoku, D., Nakamura, T., Sawano, T., Takahashi, K., & Toyanago, A. 2014, ApJ, 789, 65
Yu, H., Wang, F., Dai, Z., & Cheng, K. 2015, ApJS, 218, 13
Zhang, B., Zhang, B.-B., Virgili, F. J., et al. 2009, ApJ, 703, 1696
Zhang, F.-W., Shao, L., Yan, J.-Z., & Wei, D.-M. 2012, ApJ, 750, 88